ACS Energy LETTERS

http://pubs.acs.org/journal/aelccp

Monolithic Two-Terminal Perovskite/CIS Tandem Solar Cells with Efficiency Approaching 25%

Marco A. Ruiz-Preciado,* Fabrizio Gota, Paul Fassl, Ihteaz M. Hossain, Roja Singh, Felix Laufer, Fabian Schackmar, Thomas Feeney, Ahmed Farag, Isabel Allegro, Hang Hu, Saba Gharibzadeh, Bahram Abdollahi Nejand, Veronique S. Gevaerts, Marcel Simor, Pieter J. Bolt, and Ulrich W. Paetzold*

Cite This: *ACS Energy Lett.* 2022, 7, 2273−2281

Read Online

ACCESS | Metrics & More | Article Recommendations | Supporting Information

ABSTRACT: **Monolithic two-terminal (2T) perovskite/$CuInSe_2$ (CIS) tandem solar cells (TSCs) combine the promise of an efficient tandem photovoltaic (PV) technology with the simplicity of an all-thin-film device architecture that is compatible with flexible and lightweight PV. In this work, we present the first-ever 2T perovskite/CIS TSC with a power conversion efficiency (PCE) approaching 25% (23.5% certified, area 0.5 cm^2). The relatively planar surface profile and narrow band gap (∼1.03 eV) of our CIS bottom cell allow us to exploit the optoelectronic properties and photostability of a low-Br-containing perovskite top cell as revealed by advanced characterization techniques. Current matching was attained by proper tuning of the thickness and bandgap of the perovskite, along with the optimization of an antireflective coating for improved light in-coupling. Our study sets the baseline for fabricating efficient perovskite/CIS TSCs, paving the way for future developments that might push the efficiencies to over 30%.**

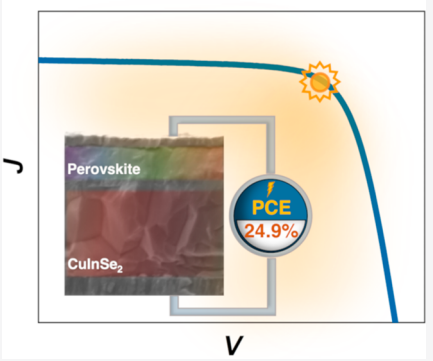

The photovoltaic (PV) market is currently dominated by single-junction devices: primarily, silicon (Si) solar cells. However, single-junction Si PV cells have matured over the decades to the point where their efficiency approaches the practical limit.[1] Nonetheless, by stacking two or more compatible solar cells in a tandem configuration, the solar spectrum can be utilized more efficiently to obtain power conversion efficiencies (PCEs) exceeding the limit of single-junction devices, which also promises a decreased levelized cost of electricity.[2,3] Thanks to their outstanding optoelectronic properties and an intense effort from the scientific community over the past decade, single-junction perovskite solar cells (PSCs) have demonstrated impressive progress, already surpassing a PCE of 25%.[4] In fact, single-junction PSCs are already rivaling established technologies such as Si and $CuIn(Ga)Se_2$ (CI(G)S).[4,5] In addition, their versatile processing routes and band gap tunability make perovskite semiconductors prime candidates for tandem PV devices, leading to a record PCE of 29.8% and 24.2% for a tandem solar cell (TSC) with a Si and CI(G)S bottom solar cell, respectively.[4] As an all-thin-film technology, perovskite/CI(G)S TSCs combine the promise of a high-efficiency tandem PV technology with the ease of a device architecture that is compatible with flexible PV and is light weight.[6−10] With the inspiration of the potential advantages of the technology, efforts to fabricate efficient two-terminal (2T) perovskite/CI(G)S TSCs started in the early stages of PSC development.[11] Notably, Han et al.[12] used a polished thick ITO layer between the CI(G)S and perovskite subcells to overcome the challenge of processing the top cell on the rough surface of the CI(G)S, achieving a certified PCE of 22.4%. Later, Albrecht and co-workers implemented a series of innovations that progressively improved the performance of 2T perovskite/CI(G)S TSCs. In their first work, they used atomic layer deposition (ALD) to conformally coat the rough bottom cell surface with a thin layer of NiO_x that, in combination with PTAA, allowed processing the top cell directly on the as-grown CI(G)S cell, achieving a PCE of 21.6%.[13] Later, they used a self-assembled monolayer (2PACz) as the hole transport layer and reached a certified PCE of 23.3%.[14] More recently, a certified PCE of 24.2% was achieved by replacing 2PACz with

Received: March 25, 2022
Accepted: April 29, 2022

https://doi.org/10.1021/acsenergylett.2c00707
ACS Energy Lett. 2022, 7, 2273−2281

Me-4PACz and using defect passivation strategies on the perovskite top cell.[15]

It is important to note that all of the aforementioned developments were performed using wide-band-gap absorbers for the top and bottom cells. However, the band gap of both the perovskite top cell and the CI(G)S bottom cell can be tuned by engineering of their composition.[16−18] This versatility is very useful when it comes to monolithic 2T TSCs with two series-interconnected subcells that require matched current generation in the top and bottom cells to maximize the power output. In this regard, a detailed balance analysis for 2T TSCs indicates that high efficiencies are possible when the band gaps of the bottom and top absorbers are varied within a certain range, with absolute optimal values at 0.94 eV for the bottom cell and ca. 1.60 eV for the top cell.[3,19−22] Critically, the band gap of CI(G)S can be reduced to close to 1 eV by drastically decreasing the gallium content in the composition of the material in a graded fashion along the layer. This composition is commonly referred to as $CuInSe_2$ (CIS), and single-junction solar cells based on it have already been reported showing PCEs over 19%.[17] Therefore, in a 2T tandem configuration, CIS perfectly pairs with the best-performing p−i−n PSCs to date, in which the perovskite absorber has a band gap slightly below 1.6 eV.[3,20,21,23] Despite that, research on perovskite/CIS TSCs is scarce and has mostly focused on four-terminal configurations[17,18] or optical simulations of 2T TSCs.[24] To the best of our knowledge, there is only one previous experimental report on 2T perovskite/CIS TSCs,[25] and the PCE was limited to ∼11%.

In this work, we present highly efficient 2T perovskite/CIS TSCs for the first time. By optimizing the semitransparent perovskite top cell when it is interconnected in tandem with a narrow-band-gap CIS bottom cell, we obtain tandem PV devices approaching a PCE of 25%. We report on improvements in light management, addressing antireflective coatings along with band-gap tuning to achieve current matching between the subcells. We also discuss further the benefits of using a CIS absorber with a narrow band gap of ca. 1.03 eV for the bottom cell, which allows us to take advantage of the excellent optoelectronic properties and phase stability of perovskites with band gaps below 1.60 eV. Our study demonstrates that perovskite/CIS TSCs have the potential to reach PCEs exceeding our current results, paving the way for future developments that might push the efficiencies over the 30% threshold.

In 2T tandem devices, the constituting top and bottom solar cells are usually connected in series, leading to an addition of the generated voltages and a recombination of the photogenerated currents of each subcell at the junction. Thus, in order to maximize the current generation of a 2T TSC, the photocurrents of the top and bottom solar cells need to match. Failing to do so will cause the overall tandem photocurrent to be limited to that of the subcell generating the smaller current. Here it should be noted that a slightly imbalanced short-circuit current density (J_{SC}) can increase the fill factor (FF) of a tandem device, partially compensating the loss in PCE due to a smaller J_{SC} value.[26,27] In order to match currents, the first step is to identify a suitable combination of band gaps for the top and bottom cells. We performed computational simulations using the open-source modeling platform EYcalc[28,29] to model the performance of 2T TSCs for different band-gap combinations. The simulations take the champion perovskite/CI(G)S TSC reported in this work (PCE of 24.9%) as a reference point. Details concerning the calculations are provided in the Supporting Information. A fit to our experimental external quantum efficiency (EQE) and an optical loss analysis can be found in Figure S1. On the basis of our simulations, the contour plot of Figure 1 shows the maximum PCE for a 2T TSC with a given combination of band gaps for the top (perovskite) and bottom (CI(G)S) absorbers. According to our model, it is possible to achieve PCEs of up to 25% for a wide range of band-gap combinations, i.e., ∼0.95−1.15 eV for the bottom cell and ∼1.54−1.72 eV for the top cell. This is in good agreement with detailed balance limit calculations for 2T TSCs.[3] As was stated before, the band gap of CI(G)S can be tuned in the range of ∼1−1.2 eV, where the most efficient single-junction CI(G)S solar cell to date has a band gap of ca. 1.08 eV.[16] Our model shows that 1.08 eV for the bottom cell is within a band-gap range that can produce a high-efficiency 2T tandem device in combination with a suitable top cell (Figure 1). However, to achieve the highest possible performance, the band gap of the CI(G)S should be further decreased to fit within the optimal range (∼0.95−1.03 eV), while the perovskite should be engineered to appropriately pair with the chosen band gap of CI(G)S (∼1.56−1.66 eV). It should be noted that, for highly luminescent perovskite top cells, a correction to lower band-gap energies should be considered for the top absorber due to luminescent coupling.[30,31] Jošt et al.[15,32] reported on the recent record 2T perovskite/CI(G)S TSC having an architecture very similar to that in this work with a certified efficiency of 24.2% for a band gap combination of ∼1.13 and ∼1.68 eV for the CI(G)S and perovskite, respectively. The PCE obtained from our simulations matches their experimental result well for this band-gap combination. Moreover, our model suggests that by decreasing the band gap of the top and bottom absorbers by ∼100 meV, while the same electronic quality of the materials is maintained, higher efficiencies can be achieved. For this, a CIS

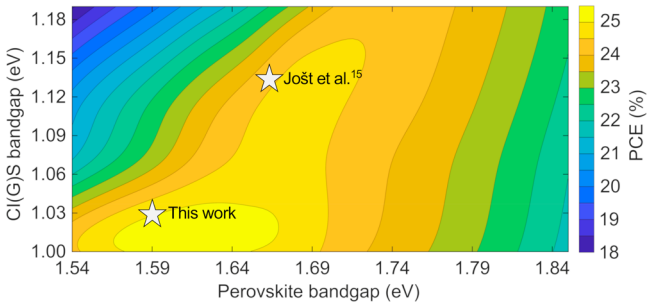

Figure 1. Contour plot showing the maximum PCE of perovskite/CI(G)S 2T tandem solar cells as a function of CI(G)S and perovskite band gap. The simulations take the 24.9% perovskite/CIS TSC introduced in this work as a reference from an optical and electrical point of view. Figure S1 shows the optical response (EQE, reflectance) of the reference cell and the corresponding simulated values. The layer thicknesses are fixed for all band-gap combinations. In particular, the perovskite thickness is set to 600 nm. The electrical parameters of the subcells for all of the CI(G)S and perovskite band gaps were adjusted so that the V_{OC}/qE_g ratio and the FF are equal for different band gaps. In particular, the V_{OC}/qE_g ratio of the perovskite cells is set to 68% and the FF to 78%, while for the CI(G)S cells the V_{OC}/qE_g ratio is 52% and the FF is 65%. Further information about the simulations can be found in the Computational Simulations section of the Supporting Information.

https://doi.org/10.1021/acsenergylett.2c00707
ACS Energy Lett. 2022, 7, 2273−2281

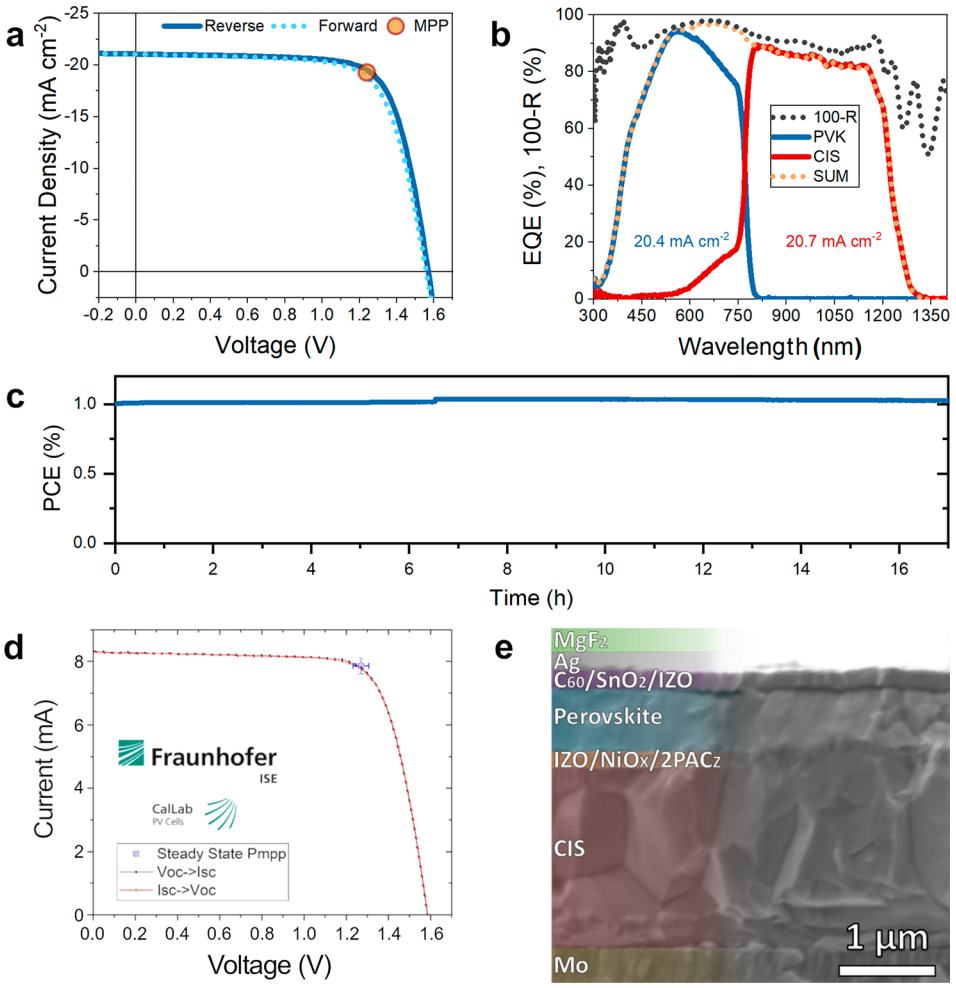

Figure 2. (a) Current density–voltage (J–V) curve for the champion tandem device. The PV parameters for this device in the reverse scan are V_{OC} = 1.57 V, J_{SC} = 21.1 mA cm^{-2}, FF = 75.2% and PCE = 24.9%. (b) EQE of the same champion device. The integrated photocurrents obtained from EQE for the top and bottom subcells are 20.4 and 20.7 mA cm^{-2}, respectively. (c) MPPT of a 2T TSC under continuous illumination at 1 sun for 17 h. (d) Current–voltage (I–V) curve of a tandem device certified at CalLab Fraunhofer ISE with a PCE of 23.5% (see the calibration certificate for Device 1 in the Supporting Information for more details). (e) Cross-sectional image and illustration of the layer stack of a 2T TSC obtained by SEM.

bottom cell with a band gap closer to 1 eV in conjunction with a perovskite top cell with a band gap of ca. 1.60 eV should be considered. In this way, PCEs of over 25% should be feasible.

By coupling a low-Ga-containing CIS (~1.03 eV) and a triple-cation perovskite (~1.59 eV) in a 2T tandem configuration, we have fabricated high-performing 2T tandem PV devices. The band gaps are determined from the inflection point of the EQE (see Figure S2).[33] A champion PCE of 24.9% was measured in house with an open-circuit voltage (V_{OC}), J_{SC}, and FF of 1.57 V, 21.1 mA cm^{-2} and 75.2%, respectively. Figure 2a shows the current density–voltage (J–V) curve, and statistics for 25 devices are provided in Figure S3. In Figure 2c we display the maximum power point tracking (MPPT) of a 2T TSC exposed to continuous illumination at 1 sun for 17 h, where the device exhibits no decrease in PCE. Figure 2b shows the EQE for the champion device that exhibits nearly perfect current matching, with the photocurrent of the TSC being only slightly limited by the perovskite top cell. The integrated photocurrents (J_{EQE}) are 20.4 and 20.7 mA cm^{-2} for the top and bottom cells, respectively.

We sent out various 2T TSCs for certification, and Figure 2d shows the current–voltage (I–V) curve for the device with the highest certified PCE of 23.5%, V_{OC} of 1.59 V, J_{SC} of 19.4 mA cm^{-2}, and FF of 75.5%. For clarification, we note that the champion device in Figure 2a,b is not the same as the best certified device in Figure 2d. To corroborate the accuracy of our in-house measurements, we compare the PV parameters and J_{EQE} values obtained from both in-house and certified measurements at CalLab Fraunhofer ISE for three different TSCs (Table S1). In all cases, the discrepancy between the in-house and certified measurements lies within a 5% margin, validating the reliability of our measurements. We note that we employ a class AAA LED solar simulator that matches the AM1.5G spectrum very well over the complete relevant spectral range (Figure S4). The corresponding calculated spectral mismatches for the top perovskite cell, the bottom CIS cell, and a single-junction CIS cell (using the EQE spectra shown in Figure 2b and Figure S5) are less than 0.5%, 5%, and 3%, respectively, emphasizing the good suitability of our solar simulator spectrum to measure 2T perovskite/CIS TSCs.

An antireflective coating (ARC) was used to improve the light in-coupling and increase the overall photocurrent. The optimization process for the ARC is described in detail in Figure S6, and the full layer stack and layout for our 2T

https://doi.org/10.1021/acsenergylett.2c00707
ACS Energy Lett. 2022, 7, 2273–2281

Table 1. Photovoltaic Parameters of the Solar Cells Presented in This Work[a]

	V_{OC} (V)	FF (%)	J_{SC} (mA cm^{-2})	PCE (%)
10%-Br PVK single junction	1.14 (1.14)	80.2 (77.6)	22.6 (22.6)	20.7 (19.9)
23%-Br PVK single junction	1.16 (1.17)	80.0 (77.5)	20.8 (20.7)	19.4 (18.7)
CIS single junction	0.532	71.2	38.8	14.7
PVK(10%-Br)/CIS 2T TSC	1.57 (1.57)	75.2 (73.6)	21.1 (21.0)	24.9 (24.3)
PVK(10%-Br)/CIS 2T TSC[b]	1.59 (1.59)	75.5 (75.0)	19.4 (19.4)	23.5

[a]Forward scan values are given in parentheses. [b]Certified at CalLab Fraunhofer ISE.

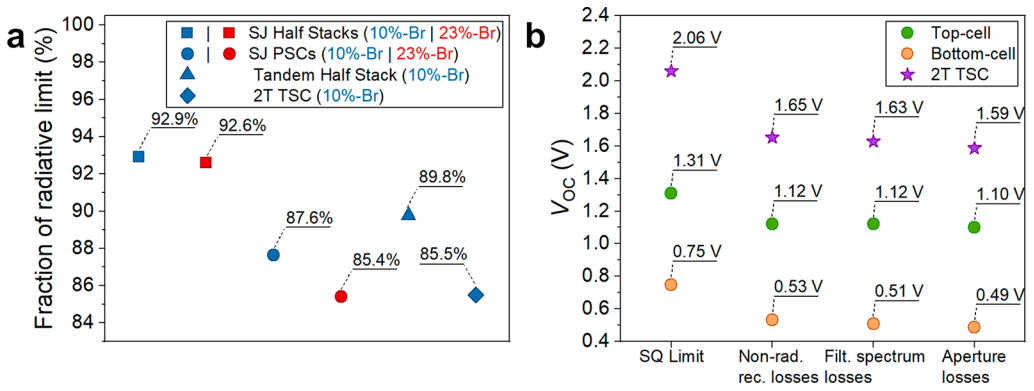

Figure 3. (a) Fraction of the radiative limit for the implied V_{OC} values of different single-junction (10%-Br and 23%-Br perovskite) and tandem (10%-Br perovskite) stacks. (b) Expected V_{OC} losses due to nonradiative recombination, the filtered spectrum (for the bottom cell), and the aperture for the top and bottom cells in a 2T perovskite/CIS TSC.

perovskite/CIS TSCs are depicted in Figure 2e and Figure S7, respectively. The hole transport layer of the top cell is formed by a very thin layer of NiO_x (15 nm) and a self-assembled monolayer of 2PACz.[14,34,35] Given that our perovskite contains methylammonium, the purpose of the NiO_x layer is to effectively isolate the perovskite layer from the intrinsic ZnO (i-ZnO) buffer layer of the CIS bottom cell to avoid the degradation of methylammonium by reaction with ZnO.[36,37]

The high performance of our 2T TSCs is a result of the high quality of the subcells, as was apparent from independent $J-V$ curves and EQEs of perovskite and CIS single-junction devices (Figure S5), as well as an appropriate optical and electrical coupling. A comparison between semitransparent single-junction PSCs with areas of 0.1 and 0.5 cm^2 is displayed in Figure S8 to show that increasing the device active area has a limited effect on the FF. To better assess the optoelectronic quality of our perovskite top cell, we compare the performance of our narrow-band-gap PSC ($Cs_{0.05}MA_{0.1}FA_{0.85}Pb(I_{0.9}Br_{0.1})_3$, $E_g \approx 1.59$ eV) from Figure S5 to that of a wider-band-gap PSC ($Cs_{0.05}MA_{0.22}FA_{0.73}Pb(I_{0.77}Br_{0.23})_3$, $E_g \approx 1.68$ eV), as shown in Figure S9. We chose the latter because it is a very popular composition used in previous reports of high-performing 2T TSCs.[14,32,34] For simplicity, further on we will refer to the narrow- and wide-band-gap compositions as 10%-Br and 23%-Br perovskites, respectively, referring to the bromide fraction relative to iodide. The PV parameters of opaque single-junction PSCs for both compositions are summarized in Table 1. Even though both compositions yield high-performing PV cells, the devices with 10%-Br exhibit a slightly higher PCE that is due to its higher V_{OC} value relative to the radiative limit.[33] Typically, a larger bromide fraction has been correlated to the formation of vacancies and defects in the perovskite bulk (i.e., a lower optoelectronic quality) together with an enhanced interface recombination for wider-band-gap PSCs, both limiting the performance.[38−40] We further analyze the optoelectronic quality and related voltage losses of our single-junction and tandem devices by calculating the implied V_{OC} value with respect to the radiative limit from photoluminescence quantum yield (PLQY) measurements at ∼1 sun for various device stacks (see Figure S10).[33,41] For single-junction half-stacks up to the perovskite layer, both 10%-Br and 23%-Br show very high implied V_{OC} values that are above 92% of the radiative limit for the respective band gap (Figure 3a). In a tandem half-stack (10%-Br) this value only slightly decreases to 89.8%, possibly due to a reduction in light out-coupling.[42] Upon completion of the single-junction PSCs with the top electrodes (C_{60}/BCP/Ag), the implied V_{OC} value is strongly decreased to 87.6% and 85.4% of the radiative limit for the 10%-Br and 23%-Br perovskites, respectively. Similarly, after completion of the 2T TSC (10%-Br), the value decreases to 85.5%. This shows that the perovskite/electron transport layer is the performance-limiting interface, as reported previously.[23,43] However, the implied V_{OC} value with respect to the radiative limit is slightly higher for 10%-Br in comparison to 23%-Br, in line with the single-junction device results discussed above. From time-resolved PL measurements we obtained a longer charge carrier lifetime for 10%-Br, which also implies a higher optoelectronic quality over 23%-Br (Figure S11). Additionally, we have determined the expected V_{OC} losses of our 2T TSCs due to nonradiative recombination, the filtered spectrum (for the bottom cell), and the aperture,[44] while considering a temperature of 25 °C. Thereby, we calculate a V_{OC} value of ∼1.10 V from the top cell and ∼0.49 V from the bottom cell, adding up to a V_{OC} value of ∼1.59 V in a 2T TSC (see Figure 3b). This matches very well the V_{OC} value measured at CalLab Fraunhofer ISE (shown in Figure 2d and denoted Device 1 in Table S1). We note that for higher temperatures additional losses must be considered, leading to expected V_{OC} drops of ∼2.04 and ∼1.32 mV °C^{-1} for the CIS[45] bottom cell and the perovskite[44] top cell, respectively,

https://doi.org/10.1021/acsenergylett.2c00707
ACS Energy Lett. 2022, 7, 2273−2281

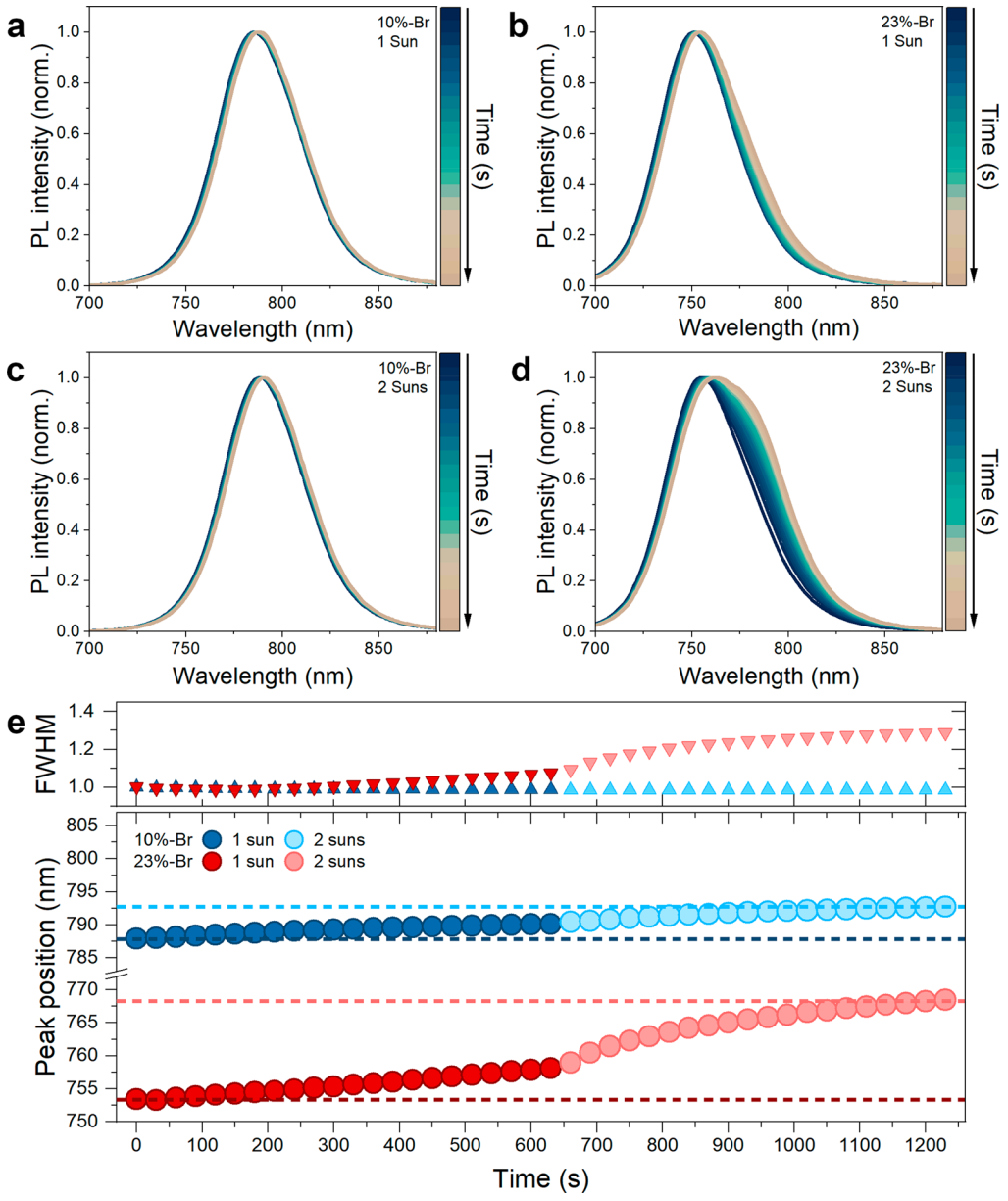

Figure 4. Photoluminescence (PL) emission spectra at the irradiation equivalent of 1 sun for (a) 10%-Br and (b) 23%-Br. PL emission spectra at the irradiation equivalent of 2 suns for (c) 10%-Br and (d) 23%-Br. (e) Representation of the PL peak displacement over time. The change in FWHM of the PL spectrum is shown normalized to the initial value. The samples were irradiated at 1 sun for 630 s followed by irradiation at 2 suns on the same spot. The spectra were collected every 30 s. The samples were kept under a N_2 atmosphere for the duration of the experiment.

which could explain the differences in measured V_{OC} values observed for the devices presented in Table S1. Details on the calculation of V_{OC} losses are provided in the Supporting Information.

In addition to higher PCEs, the 10%-Br perovskite is expected to also display better phase stability in comparison to the 23%-Br counterpart.[34,38,46] Therefore, we performed steady-state photoluminescence (PL) measurements on both 10%-Br and 23%-Br perovskites. In order to study the extent of phase segregation under device-relevant conditions, we first irradiate samples with the device stack ITO/NiO_x/2PACz/perovskite at ~1 sun intensity for 10 min, followed by another 10 min at ~2 suns using an ~525 nm laser diode. The samples were placed under a N_2 atmosphere during the experiment to avoid any influence of the environment.[47,48] The results are summarized in Figure 4. The PL spectrum of the 10%-Br perovskite exhibits only a very slight change at both 1 and 2 suns with the peak position shifting by roughly 5 nm while the PL spectral shape and full-width at half-maximum (fwhm) remain very similar (see Figure 4e). This minor peak shift has been observed before, and it is reversible when the samples are stored in the dark.[49,50] While its origin is not completely clear at this point, we do not associate it with phase segregation, considering the small amount of bromide and narrow band gap of our perovskite. On the other hand, not only does the 23%-Br perovskite exhibit a similar shift at the high-energy side of the PL spectrum but it also displays an additional asymmetric broadening of the peak that is more prominent at the low-energy side and increases over time. This asymmetric broadening is already noticeable at 1 sun, characterized by a

https://doi.org/10.1021/acsenergylett.2c00707
ACS Energy Lett. 2022, 7, 2273−2281

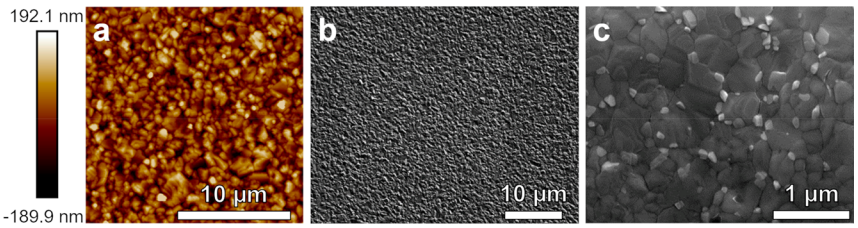

Figure 5. a Surface analysis of a CIS thin film performed by AFM. SEM surface image of b CIS, c 10%-Br perovskite layer deposited on CIS.

slight increase in the fwhm (Figure 4e), while upon illumination at 2 suns, the deformation becomes even more pronounced with the appearance of a clear shoulder at the low-energy side that results in an even stronger increase of the fwhm. This observation can be attributed to phase segregation, resulting in the formation of two different photoactive phases, one of them being an iodide-rich narrow-band-gap phase.[39,40,51,52] To investigate whether the intrinsic phase stability characteristics revealed by PL have an effect on the device stability, we performed MPPT of single-junction PSCs (Figure S12) and 2T TSCs (Figure 2c and Figure S12) under continuous illumination at 1 sun for periods of 20 and 17 h, respectively. In all cases the PCE is very stable over the duration of the experiment. However, both kinds of single-junction PSCs denote distinctive behavior during the initial phase of MPPT, with the 10%-Br increasing slightly from 19.5% to 20.0% within the first 60 min, while the PCE of the 23%-Br decreases from 19.0% to 18.3%. The latter findings could correlate with our observations from PL spectra that reveal intrinsic phase instability of the 23%-Br perovskite and are in line with the work of Peña-Camargo et al.,[39] where higher V_{OC} loss and phase instability for higher-Br-containing triple cation perovskites was demonstrated. Al-Ashouri et al. have previously investigated phase segregation in wide-band-gap triple-cation perovskites and found that slow charge extraction and poor interfacial defect passivation lead to a more pronounced photoinstability.[34] Additionally, Farooq et al. tested the influence of bias conditions on device performance under continuous illumination and concluded that maintaining the devices under open-circuit conditions accelerates device degradation.[53] These two related studies might explain the rather fast phase segregation revealed by PL (measured under open-circuit conditions without the top electrodes) and the stable performance observed under MPPT (where charges are being constantly extracted) for the 23%-Br perovskite. Nevertheless, we point out that, even if charge extraction decelerates phase segregation on the time scales considered in our experiments, we cannot exclude that it will not influence device degradation over long-term operation. Overall, this set of experiments emphasizes that the narrow-band-gap 10%-Br perovskite displays superior intrinsic phase stability in comparison to the wider-band-gap 23% perovskite under device-relevant conditions.

Fabricating 2T TSCs comes with many challenges that are not restricted to the optical and electrical coupling of the constituent layers. One of the main challenges is inherent to the morphology of the substrates and to the employed deposition techniques. Textured and rough surfaces commonly found in Si and CI(G)S solar cells have proven difficult to conformally coat with solution-processed layers.[54,55] In this regard, atomic force microscopy (AFM) reveals that a CI(G)S sample has a root-mean-square roughness (R_{RMS}) of ∼120 nm and a peak to valley distance of ∼560 nm (Figure S13). In comparison, AFM shows that our narrow-band-gap CIS has a uniform surface profile (Figure 5a,b) with $R_{RMS} \approx 53$ nm and a maximum peak to valley distance of ∼270 nm (Figure S13). These surface characteristics facilitate the processing of the perovskite top cell on the as-grown CIS bottom cell and prevent the presence of defects and shunts due to uneven coverage of the substrate's profile (see PL imaging results in Figure S14) while also avoiding the need for exceptionally thick perovskite layers.[54,55] Indeed, after optimization for current matching, conformal coverage of the CIS bottom cell was achieved with a perovskite layer of approximately 600 nm (see Figure 5c), as can also be seen in the scanning electron microscope (SEM) cross-sectional image of Figure 2e.

In summary, we present for the first time 2T perovskite/CIS TSCs with PCEs approaching 25% and a certified PCE of 23.5%. We achieve our remarkable PCEs by appropriately selecting the absorber band gaps and optimizing the perovskite thickness using a computational model as a guide. We demonstrate high performance by using a narrow-band-gap CIS as the bottom cell and a low-Br-containing perovskite as the top cell of a 2T tandem PV device. In this way, we minimize the V_{OC} losses of the perovskite top cell associated with high Br content and improve the intrinsic phase photostability of the device by decreasing phase segregation. We show that the morphological characteristics of the as-deposited CIS bottom cell permit the full coverage of the CIS substrate with the perovskite layer by a solution process (i.e., spin-coating) and that, together with the optimization of the subsequent layers, minimal V_{OC} and FF losses are possible. Our results demonstrate the potential of perovskite/CIS TSCs as a key energy solution, in particular for applications that might require flexible and/or lightweight PV devices, and open the way for future developments that may push the performances over the 30% threshold.

■ ASSOCIATED CONTENT

Supporting Information

The Supporting Information is available free of charge at https://pubs.acs.org/doi/10.1021/acsenergylett.2c00707.

Materials and sample fabrication procedures, characterizations, and computational simulations, data on simulated external quantum efficiency and reflectance, simulated layer-resolved absorptance, band-gap determination, single-junction device $J-V$ characteristics, and external quantum efficiency, steady-state and time-resolved photoluminescence, photoluminescence quantum yield, antireflective coating optimization, atomic force microscopy, photoluminescence imaging, and device calibration certificates issued by CalLab Fraunhofer ISE (PDF)

https://doi.org/10.1021/acsenergylett.2c00707
ACS Energy Lett. 2022, 7, 2273−2281

AUTHOR INFORMATION

Corresponding Authors

Marco A. Ruiz-Preciado − *Institute of Microstructure Technology, Karlsruhe Institute of Technology, 76344 Eggenstein-Leopoldshafen, Germany; Light Technology Institute, Karlsruhe Institute of Technology, 76131 Karlsruhe, Germany;* orcid.org/0000-0003-2178-5866; Email: marco-ruiz.preciado@kit.edu

Ulrich W. Paetzold − *Institute of Microstructure Technology, Karlsruhe Institute of Technology, 76344 Eggenstein-Leopoldshafen, Germany; Light Technology Institute, Karlsruhe Institute of Technology, 76131 Karlsruhe, Germany;* orcid.org/0000-0002-1557-8361; Email: ulrich.paetzold@kit.edu

Authors

Fabrizio Gota − *Institute of Microstructure Technology, Karlsruhe Institute of Technology, 76344 Eggenstein-Leopoldshafen, Germany; Light Technology Institute, Karlsruhe Institute of Technology, 76131 Karlsruhe, Germany*

Paul Fassl − *Institute of Microstructure Technology, Karlsruhe Institute of Technology, 76344 Eggenstein-Leopoldshafen, Germany; Light Technology Institute, Karlsruhe Institute of Technology, 76131 Karlsruhe, Germany;* orcid.org/0000-0002-9604-3405

Ihteaz M. Hossain − *Institute of Microstructure Technology, Karlsruhe Institute of Technology, 76344 Eggenstein-Leopoldshafen, Germany; Light Technology Institute, Karlsruhe Institute of Technology, 76131 Karlsruhe, Germany;* orcid.org/0000-0001-6533-1757

Roja Singh − *Institute of Microstructure Technology, Karlsruhe Institute of Technology, 76344 Eggenstein-Leopoldshafen, Germany; Light Technology Institute, Karlsruhe Institute of Technology, 76131 Karlsruhe, Germany;* orcid.org/0000-0002-2202-3612

Felix Laufer − *Institute of Microstructure Technology, Karlsruhe Institute of Technology, 76344 Eggenstein-Leopoldshafen, Germany; Light Technology Institute, Karlsruhe Institute of Technology, 76131 Karlsruhe, Germany*

Fabian Schackmar − *Institute of Microstructure Technology, Karlsruhe Institute of Technology, 76344 Eggenstein-Leopoldshafen, Germany; Light Technology Institute, Karlsruhe Institute of Technology, 76131 Karlsruhe, Germany*

Thomas Feeney − *Institute of Microstructure Technology, Karlsruhe Institute of Technology, 76344 Eggenstein-Leopoldshafen, Germany; Light Technology Institute, Karlsruhe Institute of Technology, 76131 Karlsruhe, Germany*

Ahmed Farag − *Institute of Microstructure Technology, Karlsruhe Institute of Technology, 76344 Eggenstein-Leopoldshafen, Germany; Light Technology Institute, Karlsruhe Institute of Technology, 76131 Karlsruhe, Germany*

Isabel Allegro − *Light Technology Institute, Karlsruhe Institute of Technology, 76131 Karlsruhe, Germany;* orcid.org/0000-0001-9663-4910

Hang Hu − *Institute of Microstructure Technology, Karlsruhe Institute of Technology, 76344 Eggenstein-Leopoldshafen, Germany; Light Technology Institute, Karlsruhe Institute of Technology, 76131 Karlsruhe, Germany;* orcid.org/0000-0001-8141-8772

Saba Gharibzadeh − *Institute of Microstructure Technology, Karlsruhe Institute of Technology, 76344 Eggenstein-Leopoldshafen, Germany; Light Technology Institute, Karlsruhe Institute of Technology, 76131 Karlsruhe, Germany*

Bahram Abdollahi Nejand − *Institute of Microstructure Technology, Karlsruhe Institute of Technology, 76344 Eggenstein-Leopoldshafen, Germany; Light Technology Institute, Karlsruhe Institute of Technology, 76131 Karlsruhe, Germany*

Veronique S. Gevaerts − *TNO Partner in Solliance, Department of Solar Technology and Applications, NL-5656 AE Eindhoven, The Netherlands;* orcid.org/0000-0003-2281-522X

Marcel Simor − *TNO Partner in Solliance, Department of Solar Technology and Applications, NL-5656 AE Eindhoven, The Netherlands*

Pieter J. Bolt − *TNO Partner in Solliance, Department of Solar Technology and Applications, NL-5656 AE Eindhoven, The Netherlands*

Complete contact information is available at: https://pubs.acs.org/10.1021/acsenergylett.2c00707

Author Contributions

The manuscript was prepared by M.A.R-P. with support from U.W.P. and P.F. through contributions from all authors. M.A.R-P. coordinated the development of the study and performed most of the laboratory work. S.G. supported M.A.R-P. on the fabrication of PV devices. T.F. and H.H. deposited SnO_2 layers by ALD on TSCs and semitransparent SJ PSCs. F.G. performed the device modeling. I.M.H. and I.A. did ss-PL and tr-PL measurements. P.F. carried out absolute PL measurements. F.L. and F.S. helped with PL and EL imaging. A.F. and B.A.N. took SEM images. R.S. performed MPPT measurements. V.S.G., M.S. and P.J.B. provided the CIS bottom cells and contributed with their expertise on $CuInSe_2$ solar cells. U.W.P. conceived and directed the study.

Notes

The authors declare no competing financial interest.

ACKNOWLEDGMENTS

The authors are grateful for funding from the European Union's Horizon 2020 research and innovation program under grant agreement no. 850937 (PERCISTAND), the Federal ministry of energy and economics (CAPITANO, funding code 03EE1038B), the Initiating and Networking funding of the Helmholtz Association HYIG of U.W.P. (VH-NG-1148), the Helmholtz Energy Materials Foundry (HEMF), and Karlsruhe School of Optics and Photonics (KSOP). The authors received further support from the Helmholtz Association Program: Program oriented funding IV, Materials and Technologies for the Energy Transition, Topic 1: Photovoltaics and Wind Energy, Code: 38.01.03. The authors acknowledge the Karlsruhe Nano Micro Facility (KNMF) at KIT for allowing the use of the ALD system. H.H. is thankful to the Chinese Scholarship Council (CSC, no. 201808420221) for funding his doctoral research work. B.A.N. acknowledges the financial support from the European Union's Horizon 2020 research and innovation program under the Marie Skłodowska-Curie grant agreement no. 840937. The authors thank Dr. Stefan

https://doi.org/10.1021/acsenergylett.2c00707
ACS Energy Lett. 2022, 7, 2273−2281

Paetel from the Center for Solar Energy and Hydrogen Research of Baden-Württemberg, Germany (ZSW), for providing CI(G)S samples for AFM surface analysis and PL imaging (shown in Figure S13s and S14). The authors are deeply grateful to our colleague Pieter Jan, or just Pieter internationally, who passed away in December 2021 during the preparation of this paper. Pieter was always passionate about new photovoltaic technologies and contributed extensively to this project. He was well-known and respected for his international collaborations such as the PERCISTAND project. We will remember Pieter as a highly intelligent, passionate, and friendly colleague. We sorely miss you!

REFERENCES

(1) Richter, A.; Hermle, M.; Glunz, S. W. Reassessment of the Limiting Efficiency for Crystalline Silicon Solar Cells. *IEEE J. Photovoltaics* **2013**, *3* (4), 1184−1191.

(2) Kost, C.; Shammugam, S.; Jülch, V.; Nguyen, H.-T.; Schlegl, T. *Levelized Cost of Electricity - Renewable Energy Technologies*; Fraunhofer Institut für Solare Energiesysteme ISE: 2018.

(3) de Vos, A. Detailed Balance Limit of the Efficiency of Tandem Solar Cells. *J. Phys. D. Appl. Phys.* **1980**, *13* (5), 839−846.

(4) NREL. Best Research-Cell Efficiency Chart. Photovoltaic Research. https://www.nrel.gov/pv/cell-efficiency.html (accessed March 2022).

(5) Min, H.; Lee, D. Y.; Kim, J.; Kim, G.; Lee, K. S.; Kim, J.; Paik, M. J.; Kim, Y. K.; Kim, K. S.; Kim, M. G.; Shin, T. J.; Il Seok, S. Perovskite Solar Cells with Atomically Coherent Interlayers on SnO2 Electrodes. *Nature* **2021**, *598*, 444−450.

(6) Jošt, M.; Kegelmann, L.; Korte, L.; Albrecht, S. Monolithic Perovskite Tandem Solar Cells: A Review of the Present Status and Advanced Characterization Methods Toward 30% Efficiency. *Adv. Energy Mater.* **2020**, *10*, 1904102.

(7) Jesper Jacobsson, T.; Correa-Baena, J. P.; Pazoki, M.; Saliba, M.; Schenk, K.; Grätzel, M.; Hagfeldt, A. Exploration of the Compositional Space for Mixed Lead Halogen Perovskites for High Efficiency Solar Cells. *Energy Environ. Sci.* **2016**, *9* (5), 1706−1724.

(8) Correa-Baena, J. P.; Abate, A.; Saliba, M.; Tress, W.; Jesper Jacobsson, T.; Grätzel, M.; Hagfeldt, A. The Rapid Evolution of Highly Efficient Perovskite Solar Cells. *Energy Environ. Sci.* **2017**, *10* (3), 710−727.

(9) Lang, F.; Jošt, M.; Frohna, K.; Köhnen, E.; Al-Ashouri, A.; Bowman, A. R.; Bertram, T.; Morales-Vilches, A. B.; Koushik, D.; Tennyson, E. M.; Galkowski, K.; Landi, G.; Creatore, M.; Stannowski, B.; Kaufmann, C. A.; Bundesmann, J.; Rappich, J.; Rech, B.; Denker, A.; Albrecht, S.; Neitzert, H. C.; Nickel, N. H.; Stranks, S. D. Proton Radiation Hardness of Perovskite Tandem Photovoltaics. *Joule* **2020**, *4* (5), 1054−1069.

(10) Fu, F.; Nishiwaki, S.; Werner, J.; Feurer, T.; Pisoni, S.; Jeangros, Q.; Buecheler, S.; Ballif, C.; Tiwari, A. N. Flexible Perovskite/Cu(In,Ga)Se2Monolithic Tandem Solar Cells. *aRXIV* 2019. DOI: 10.48550/arxiv.1907.10330.

(11) Todorov, T.; Gershon, T.; Gunawan, O.; Lee, Y. S.; Sturdevant, C.; Chang, L.-Y.; Guha, S. Monolithic Perovskite-CIGS Tandem Solar Cells via In Situ Band Gap Engineering. *Adv. Energy Mater.* **2015**, *5* (23), 1500799.

(12) Han, Q.; Hsieh, Y.-T.; Meng, L.; Wu, J.-L.; Sun, P.; Yao, E.-P.; Chang, S.-Y.; Bae, S.-H.; Kato, T.; Bermudez, V.; Yang, Y. High-Performance Perovskite/Cu(In,Ga)Se2Monolithic Tandem Solar Cells. *Science* **2018**, *361* (6405), 904−908.

(13) Jošt, M.; Bertram, T.; Koushik, D.; Marquez, J. A.; Verheijen, M. A.; Heinemann, M. D.; Köhnen, E.; Al-Ashouri, A.; Braunger, S.; Lang, F.; Rech, B.; Unold, T.; Creatore, M.; Lauermann, I.; Kaufmann, C. A.; Schlatmann, R.; Albrecht, S. 21.6%-Efficient Monolithic Perovskite/Cu(In,Ga)Se2 Tandem Solar Cells with Thin Conformal Hole Transport Layers for Integration on Rough Bottom Cell Surfaces. *ACS Energy Lett.* **2019**, *4* (2), 583−590.

(14) Al-Ashouri, A.; Magomedov, A.; Roß, M.; Jošt, M.; Talaikis, M.; Chistiakova, G.; Bertram, T.; Márquez, J. A.; Köhnen, E.; Kasparavičius, E.; Levcenco, S.; Gil-Escrig, L.; Hages, C. J.; Schlatmann, R.; Rech, B.; Malinauskas, T.; Unold, T.; Kaufmann, C. A.; Korte, L.; Niaura, G.; Getautis, V.; Albrecht, S. Conformal Monolayer Contacts with Lossless Interfaces for Perovskite Single Junction and Monolithic Tandem Solar Cells. *Energy Environ. Sci.* **2019**, *12* (11), 3356−3369.

(15) Jošt, M.; Köhnen, E.; Al-Ashouri, A.; Bertram, T.; Tomšič, Š.; Magomedov, A.; Kasparavicius, E.; Kodalle, T.; Lipovšek, B.; Getautis, V.; Schlatmann, R.; Kaufmann, C. A.; Albrecht, S.; Topič, M. Perovskite/CIGS Tandem Solar Cells: From Certified 24.2% Toward 30% and Beyond. *ACS Energy Lett.* **2022**, *7*, 1298−1307.

(16) Nakamura, M.; Yamaguchi, K.; Kimoto, Y.; Yasaki, Y.; Kato, T.; Sugimoto, H. Cd-Free Cu(In,Ga)(Se,S)2 Thin-Film Solar Cell with Record Efficiency of 23.35%. *IEEE J. Photovoltaics* **2019**, *9* (6), 1863−1867.

(17) Feurer, T.; Carron, R.; Torres Sevilla, G.; Fu, F.; Pisoni, S.; Romanyuk, Y. E.; Buecheler, S.; Tiwari, A. N. Efficiency Improvement of Near-Stoichiometric CuInSe2 Solar Cells for Application in Tandem Devices. *Adv. Energy Mater.* **2019**, *9* (35), 1901428.

(18) Jiang, Y.; Feurer, T.; Carron, R.; Sevilla, G. T.; Moser, T.; Pisoni, S.; Erni, R.; Rossell, M. D.; Ochoa, M.; Hertwig, R.; Tiwari, A. N.; Fu, F. High-Mobility In2O3:H Electrodes for Four-Terminal Perovskite/CuInSe2 Tandem Solar Cells. *ACS Nano* **2020**, *14* (6), 7502−7512.

(19) Bremner, S. P.; Levy, M. Y.; Honsberg, C. B. Analysis of Tandem Solar Cell Efficiencies under AM1.5G Spectrum Using a Rapid Flux Calculation Method. *Prog. Photovoltaics Res. Appl.* **2008**, *16* (3), 225−233.

(20) Minnaert, B.; Veelaert, P. Guidelines for the Bandgap Combinations and Absorption Windows for Organic Tandem and Triple-Junction Solar Cells. *Materials* **2012**, *5* (10), 1933−1953.

(21) Hörantner, M. T.; Snaith, H. J. Predicting and Optimizing the Energy Yield of Perovskite-on-Silicon Tandem Solar Cells under Real World Conditions. *Energy Environ. Sci.* **2017**, *10* (9), 1983−1993.

(22) Sadegh, F.; Akin, S.; Moghadam, M.; Keshavarzi, R.; Mirkhani, V.; Ruiz-Preciado, M. A.; Akman, E.; Zhang, H.; Amini, M.; Tangestaninejad, S.; Mohammadpoor-Baltork, I.; Graetzel, M.; Hagfeldt, A.; Tress, W. Copolymer-Templated Nickel Oxide for High-Efficiency Mesoscopic Perovskite Solar Cells in Inverted Architecture. *Adv. Funct. Mater.* **2021**, *31*, 2102237.

(23) Gharibzadeh, S.; Fassl, P.; Hossain, I. M.; Rohrbeck, P.; Frericks, M.; Schmidt, M.; Duong, T.; Khan, M. R.; Abzieher, T.; Nejand, B. A.; Schackmar, F.; Almora, O.; Feeney, T.; Singh, R.; Fuchs, D.; Lemmer, U.; Hofmann, J. P.; Weber, S. A. L.; Paetzold, U. W. Two Birds with One Stone: Dual Grain-Boundary and Interface Passivation Enables > 22% Efficient Inverted Methylammonium-Free Perovskite Solar Cells. *Energy Environ. Sci.* **2021**, *14* (11), 5875−5893.

(24) Ahangharnejhad, R. H.; Song, Z.; Phillips, A. B.; Watthage, S. C.; Almutawah, Z. S.; Sapkota, D. R.; Koirala, P.; Collins, R. W.; Yan, Y.; Heben, M. J. Optical Design of Perovskite Solar Cells for Applications in Monolithic Tandem Configuration with CuInSe2 Bottom Cells. *MRS Adv.* **2018**, *3* (52), 3111−3119.

(25) Jang, Y. H.; Lee, J. M.; Seo, J. W.; Kim, I.; Lee, D.-K. Monolithic Tandem Solar Cells Comprising Electrodeposited CuInSe2 and Perovskite Solar Cells with a Nanoparticulate ZnO Buffer Layer. *J. Mater. Chem. A* **2017**, *5*, 19439−19446.

(26) Boccard, M.; Ballif, C. Influence of the Subcell Properties on the Fill Factor of Two-Terminal Perovskite-Silicon Tandem Solar Cells. *ACS Energy Lett.* **2020**, *5* (4), 1077−1082.

(27) Köhnen, E.; Jošt, M.; Morales-Vilches, A. B.; Tockhorn, P.; Al-Ashouri, A.; Macco, B.; Kegelmann, L.; Korte, L.; Rech, B.; Schlatmann, R.; Stannowski, B.; Albrecht, S. Highly Efficient Monolithic Perovskite Silicon Tandem Solar Cells: Analyzing the Influence of Current Mismatch on Device Performance. *Sustain. Energy Fuels* **2019**, *3* (8), 1995−2005.

(28) Schmager, R.; Paetzold, U. W.; Langenhorst, M.; Gota, F.; Lehr, J. EYcalc - Energy Yield Calculator for Multi-Junction Solar

Modules with Realistic Irradiance Data and Textured Interfaces. 2021. DOI: 10.5281/zenodo.4696257.
(29) Schmager, R.; Langenhorst, M.; Lehr, J.; Lemmer, U.; Richards, B. S.; Paetzold, U. W. Methodology of Energy Yield Modelling of Perovskite-Based Multi-Junction Photovoltaics. *Opt. Express* **2019**, *27* (8), A507.
(30) Bowman, A. R.; Lang, F.; Chiang, Y.-H.; Jiménez-Solano, A.; Frohna, K.; Eperon, G. E.; Ruggeri, E.; Abdi-Jalebi, M.; Anaya, M.; Lotsch, B. v; Stranks, S. D. Relaxed Current Matching Requirements in Highly Luminescent Perovskite Tandem Solar Cells and Their Fundamental Efficiency Limits. *ACS Energy Lett.* **2021**, *6*, 612−620.
(31) Jäger, K.; Tillmann, P.; Katz, E. A.; Becker, C. Perovskite/Silicon Tandem Solar Cells: Effect of Luminescent Coupling and Bifaciality. *Sol. RRL* **2021**, *5* (3), 2000628.
(32) Jošt, M.; Al-Ashouri, A.; Lipovšek, B.; Bertram, T.; Schlatmann, R.; Kaufmann, C. A.; Topič, M.; Albrecht, S. *Perovskite/CIGS Tandem Solar Cells − Can They Catch up with Perovskite/c-Si Tandems?* In 47th IEEE Photovoltaic Specialists Conference (PVSC); Royal Society of Chemistry: 2020; Vol. *12*, pp 0763−0766.
(33) Krückemeier, L.; Rau, U.; Stolterfoht, M.; Kirchartz, T. How to Report Record Open-Circuit Voltages in Lead-Halide Perovskite Solar Cells. *Adv. Energy Mater.* **2020**, *10* (1), 1902573.
(34) Al-Ashouri, A.; Köhnen, E.; Li, B.; Magomedov, A.; Hempel, H.; Caprioglio, P.; Márquez, J. A.; Vilches, A. B. M.; Kasparavicius, E.; Smith, J. A.; Phung, N.; Menzel, D.; Grischek, M.; Kegelmann, L.; Skroblin, D.; Gollwitzer, C.; Malinauskas, T.; Jošt, M.; Matič, G.; Rech, B.; Schlatmann, R.; Topič, M.; Korte, L.; Abate, A.; Stannowski, B.; Neher, D.; Stolterfoht, M.; Unold, T.; Getautis, V.; Albrecht, S. Monolithic Perovskite/Silicon Tandem Solar Cell with > 29% Efficiency by Enhanced Hole Extraction. *Science* **2020**, *370* (6522), 1300−1309.
(35) Magomedov, A.; Al-Ashouri, A.; Kasparavičius, E.; Strazdaite, S.; Niaura, G.; Jošt, M.; Malinauskas, T.; Albrecht, S.; Getautis, V. Self-Assembled Hole Transporting Monolayer for Highly Efficient Perovskite Solar Cells. *Adv. Energy Mater.* **2018**, *8* (32), 1801892.
(36) Schutt, K.; Nayak, P. K.; Ramadan, A. J.; Wenger, B.; Lin, Y. H.; Snaith, H. J. Overcoming Zinc Oxide Interface Instability with a Methylammonium-Free Perovskite for High-Performance Solar Cells. *Adv. Funct. Mater.* **2019**, *29* (47), 1900466.
(37) An, Q.; Fassl, P.; Hofstetter, Y. J.; Becker-Koch, D.; Bausch, A.; Hopkinson, P. E.; Vaynzof, Y. High Performance Planar Perovskite Solar Cells by ZnO Electron Transport Layer Engineering. *Nano Energy* **2017**, *39*, 400−408.
(38) Xu, J.; Boyd, C. C.; Yu, Z. J.; Palmstrom, A. F.; Witter, D. J.; Larson, B. W.; France, R. M.; Werner, J.; Harvey, S. P.; Wolf, E. J.; Weigand, W.; Manzoor, S.; A M van Hest, M. F.; Berry, J. J.; Luther, J. M.; Holman, Z. C.; McGehee, M. D. Triple-Halide Wide-Band Gap Perovskites with Suppressed Phase Segregation for Efficient Tandems. *Science* **2020**, *367* (6482), 1097−1104.
(39) Peña-Camargo, F.; Caprioglio, P.; Zu, F.; Gutierrez-Partida, E.; Wolff, C. M.; Brinkmann, K.; Albrecht, S.; Riedl, T.; Koch, N.; Neher, D.; Stolterfoht, M. Halide Segregation versus Interfacial Recombination in Bromide-Rich Wide-Gap Perovskite Solar Cells. *ACS Energy Lett.* **2020**, *5* (8), 2728−2736.
(40) Mahesh, S.; Ball, J. M.; Oliver, R. D. J.; Mcmeekin, D. P.; Nayak, P. K.; Johnston, M. B.; Snaith, H. J. Revealing the Origin of Voltage Loss in Mixed-Halide Perovskite Solar Cells. *Energy Environ. Sci.* **2020**, *13*, 258−267.
(41) Stolterfoht, M.; Grischek, M.; Caprioglio, P.; Wolff, C. M.; Gutierrez-Partida, E.; Peña-Camargo, F.; Rothhardt, D.; Zhang, S.; Raoufi, M.; Wolansky, J.; Abdi-Jalebi, M.; Stranks, S. D.; Albrecht, S.; Kirchartz, T.; Neher, D. How To Quantify the Efficiency Potential of Neat Perovskite Films: Perovskite Semiconductors with an Implied Efficiency Exceeding 28%. *Adv. Mater.* **2020**, *32* (17), 2000080.
(42) Fassl, P.; Lami, V.; Berger, F. J.; Falk, L. M.; Zaumseil, J.; Richards, B. S.; Howard, I. A.; Vaynzof, Y.; Paetzold, U. W. Revealing the Internal Luminescence Quantum Efficiency of Perovskite Films via Accurate Quantification of Photon Recycling. *Matter* **2021**, *4* (4), 1391−1412.
(43) Warby, J.; Zu, F.; Zeiske, S.; Gutierrez-Partida, E.; Frohloff, L.; Kahmann, S.; Frohna, K.; Mosconi, E.; Radicchi, E.; Lang, F.; Shah, S.; Peña-Camargo, F.; Hempel, H.; Unold, T.; Koch, N.; Armin, A.; de Angelis, F.; Stranks, S. D.; Neher, D.; Stolterfoht, M. Understanding Performance Limiting Interfacial Recombination in Pin Perovskite Solar Cells. *Adv. Energy Mater.* **2022**, *12*, 2103567.
(44) Kiermasch, D.; Gil-Escrig, L.; Bolink, H. J.; Tvingstedt, K. Effects of Masking on Open-Circuit Voltage and Fill Factor in Solar Cells. *Joule* **2019**, *3* (1), 16−26.
(45) Jošt, M.; Lipovšek, B.; Glažar, B.; Al-Ashouri, A.; Brecl, K.; Matič, G.; Magomedov, A.; Getautis, V.; Topič, M.; Albrecht, S. Perovskite Solar Cells Go Outdoors: Field Testing and Temperature Effects on Energy Yield. *Adv. Energy Mater.* **2020**, *10* (25), 2000454.
(46) Bush, K. A.; Frohna, K.; Prasanna, R.; Beal, R. E.; Leijtens, T.; Swifter, S. A.; Mcgehee, M. D. Compositional Engineering for Efficient Wide Band Gap Perovskites with Improved Stability to Photoinduced Phase Segregation. *ACS Energy Lett.* **2018**, *3* (2), 428−435.
(47) Cacovich, S.; Messou, D.; Bercegol, A.; Ne, S.; Béchu, B.; Yaiche, A.; Shafique, H.; Rousset, J.; Schulz, P.; Bouttemy, M.; Lombez, L. Light-Induced Passivation in Triple Cation Mixed Halide Perovskites: Interplay between Transport Properties and Surface Chemistry. *ACS Appl. Mater. Interfaces* **2020**, *12* (31), 34784−34794.
(48) Fassl, P.; Zakharko, Y.; Falk, L. M.; Goetz, K. P.; Paulus, F.; Taylor, A. D.; Zaumseil, J.; Vaynzof, Y. Effect of Density of Surface Defects on Photoluminescence Properties in MAPbI3 Perovskite Films. *J. Mater. Chem. C* **2019**, *7*, 5285−5292.
(49) Tsai, H.; Asadpour, R.; Blancon, J.-C.; Stoumpos, C. C.; Durand, O.; Strzalka, J. W.; Chen, B.; Verduzco, R.; Ajayan, P. M.; Tretiak, S.; Even, J.; Alam, M. A.; Kanatzidis, M. G.; Nie, W.; Mohite, A. D. Light-Induced Lattice Expansion Leads to High-Efficiency Perovskite Solar Cells. *Science* **2018**, *360* (6384), 67−70.
(50) Lin, H.-J.; Cacovich, S.; Rebai, A.; Rousset, J.; Longeaud, C. Influence of Environment and Light-Stress on the Optoelectronic Properties of Triple-Cation Perovskite Thin Films. *ACS Appl. Mater. Interfaces* **2020**, *12* (17), 19495−19503.
(51) Slotcavage, D. J.; Karunadasa, H. I.; Mcgehee, M. D. Light-Induced Phase Segregation in Halide-Perovskite Absorbers. *ACS Energy Lett.* **2016**, *1* (6), 1199−1205.
(52) Knight, A. J.; Wright, A. D.; Patel, J. B.; McMeekin, D. P.; Snaith, H. J.; Johnston, M. B.; Herz, L. M. Electronic Traps and Phase Segregation in Lead Mixed-Halide Perovskite. *ACS Energy Lett.* **2019**, *4* (1), 75−84.
(53) Farooq, A.; Khan, M. R.; Abzieher, T.; Voigt, A.; Lupascu, D. C.; Lemmer, U.; Richards, B. S.; Paetzold, U. W. Photodegradation of Triple-Cation Perovskite Solar Cells: The Role of Spectrum and Bias Conditions. *ACS Appl. Energy Mater.* **2021**, *4* (4), 3083−3092.
(54) Chen, B.; Baek, S.-W.; Hou, Y.; Aydin, E.; de Bastiani, M.; Scheffel, B.; Proppe, A.; Huang, Z.; Wei, M.; Wang, Y.-K.; Jung, E.-H.; Allen, T. G.; van Kerschaver, E.; Pelayo García de Arquer, F.; Saidaminov, M. I.; Hoogland, S.; de Wolf, S.; Sargent, E. H. Enhanced Optical Path and Electron Diffusion Length Enable High-Efficiency Perovskite Tandems. *Nat. Commun.* **2020**, *11* (1), 1−9.
(55) Hou, Y.; Aydin, E.; de Bastiani, M.; Xiao, C.; Isikgor, F. H.; Xue, D.-J.; Chen, B.; Chen, H.; Bahrami, B.; Chowdhury, A. H.; Johnston, A.; Baek, S.-W.; Huang, Z.; Wei, M.; Dong, Y.; Troughton, J.; Jalmood, R.; Mirabelli, A. J.; Allen, T. G.; van Kerschaver, E.; Saidaminov, M. I.; Baran, D.; Qiao, Q.; Zhu, K.; de Wolf, S.; Sargent, E. H. Efficient Tandem Solar Cells with Solution-Processed Perovskite on Textured Crystalline Silicon. *Science* **2020**, *367* (6482), 1135−1140.

https://doi.org/10.1021/acsenergylett.2c00707
ACS Energy Lett. 2022, 7, 2273−2281